HHS Public Access

Author manuscript

Biomaterials. Author manuscript; available in PMC 2019 July 01.

Published in final edited form as:

Biomaterials. 2018 July ; 170: 26–36. doi:10.1016/j.biomaterials.2018.03.054.

Polymeric Micelles: Theranostic Co-Delivery System for Poorly Water-Soluble Drugs and Contrast Agents

Jaydev R. Upponi,
Center for Pharmaceutical Biotechnology & Nanomedicine, Department of Pharmaceutical Sciences, Northeastern University, 140 The Fenway, Boston, MA 02115, USA

Kaushal Jerajani,
Center for Pharmaceutical Biotechnology & Nanomedicine, Department of Pharmaceutical Sciences, Northeastern University, 140 The Fenway, Boston, MA 02115, USA

Dattatri K. Nagesha,
Electronic Materials Research Institute; Department of Physics, Northeastern University, 360 Huntington Ave, Boston, MA 02115, USA

Praveen Kulkarni,
Center for Translational NeuroImaging, Department of Pharmaceutical Sciences, Northeastern University, 360 Huntington Ave, Boston, MA 02115, USA

Srinivas Sridhar,
Electronic Materials Research Institute; Department of Physics, Northeastern University, 360 Huntington Ave, Boston, MA 02115, USA

Craig Ferris, and
Center for Translational NeuroImaging, Department of Pharmaceutical Sciences, Northeastern University, 360 Huntington Ave, Boston, MA 02115, USA

Vladimir P. Torchilin
Center for Pharmaceutical Biotechnology & Nanomedicine, Department of Pharmaceutical Sciences, Northeastern University, 140 The Fenway, Boston, MA 02115, USA

Abstract

Interest in theranostic agents has continued to grow because of their promise for simultaneous cancer detection and therapy. A platform-based nanosized combination agent suitable for the enhanced diagnosis and treatment of cancer was prepared using polymeric polyethylene glycol-phosphatidylethanolamine-based micelles loaded with both, poorly soluble chemotherapeutic agent paclitaxel and hydrophobic superparamagnetic iron oxide nanoparticles (SPION), a Magnetic Resonance Imaging contrast agent. The co-loaded paclitaxel and SPION did not affect

Correspondence to: Vladimir P. Torchilin.

SUPPLEMENTARY DATA

Supporting Information is available online from the Biomaterials online library or from the author.

each other's functional properties *in vitro. In vivo*, the resulting paclitaxel-SPION-co-loaded PEG-PE micelles retained their Magnetic Resonance contrast properties and apoptotic activity in breast and melanoma tumor mouse models. Such theranostic systems are likely to play a significant role in the combined diagnosis and therapy that leads to a more personalized and effective form of treatment.

Keywords

Nanoparticles; Micelles; Cancer therapy; Diagnostics; Drug Delivery; Theranostics

INTRODUCTION

For many decades, a "one size fits all" model for chemotherapy has somewhat successfully served the wide variety of cancer patients. Recently, a shift in the paradigm for cancer management has moved physicians from this model towards a more personalized medicine: the right drug for the right person, administered at the right time [1] using theranostics. The term theranostic was coined about a decade ago and used to describe diagnostic tests developed to guide personalized therapies. Recently it has referred to a fusion of diagnostic and therapeutic strategies with the rationale of increased safety and efficacy in a more personalized form [2].

Many poorly soluble anti-cancer drugs such as paclitaxel (PTX) exhibit premature degradation, undesirable side-effects and low bioavailability. These challenges have begun to be overcome using nanotechnology. Amongst the assortment of nanoassemblies available, poly (ethylene glycol)-phosphatidylethanolamine (PEG-PE) polymeric micelles represent a promising nano-system with the advantages of small size (5 to 100 nm) and especial usefulness for encapsulation of both poorly soluble drugs and contrast agents. They also exhibit prolonged circulation in blood due to the protective effect of the hydrophilic PEG chains in the micelle's outer corona. This small size and long circulation time allow accumulation in tumors and infarcted tissues due to the enhanced permeability and retention (EPR) effect, qualities that make PEG-PE micelles a nanomaterial that can serve as an effective theranostic agent [3].

Both therapy and effective diagnosis of cancer are keys for optimal treatment. The variety of contrast agents now available allows applications using imaging modalities, such as near-infrared (NIR), magnetic resonance imaging (MRI), positron emission tomography (PET), computed tomography (CT), photoacoustic imaging (PAI) and ultrasound (US) [4]. Among these, MRI is of specific interest since it offers high soft tissue contrast with high spatial resolution (~50 μm) [5]. To enhance the quality of imaging and distinguish a tumor or infarcted region from normal tissue, contrast agents are employed. The iron oxide nanoparticle (ION) is amongst the MRI contrast agents that also include chelated paramagnetic metal ions (gadolinium, manganese, dysprosium).

Within the family of IONs, the superparamagnetic iron oxide nanoparticles (SPION), such as, maghemite (γ-Fe_2O_3) or magnetite (Fe_3O_4) are available in a variety of sizes for application as MRI contrast agents [6]. SPIONs have been used in theranostic agents in

conjunction with many chemotherapeutic agents [7], and their lack of toxicity has been extensively documented [8, 9]. SPION are a prime choice for theranostic preparations due to their high magnetization values and they yield much stronger *in vivo* transverse and longitudinal relaxation effects compared to Gd-based contrast agents [10]. Additionally, in any theranostic agent, it is important to balance the imaging and diagnostic capabilities with the therapeutic efficacy of the chemotherapeutic agent. Furthermore, effective performance requires that neither agents interferes with the other's activity.

Here we report on a model PEG-PE-based polymeric micellar theranostic agent composed of SPIONs and PTX that are either poorly soluble or completely insoluble in aqueous medium. Our aim was to formulate, optimize and prepare this agent and assess both of its functional activities. We confirmed the maintenance of imaging quality with MRI and the chemotherapeutic drug activity by observing significant apoptosis in cancer cells *in vitro* and *in vivo* in murine mammary (4T1) and melanoma (B16F10) mouse models.

MATERIALS AND METHODS

Materials

1,2-Distearoyl-sn-glycero-3-phosphoethanolamine-N-[poly(ethyleneglycol)2000] (PEG2000–PE) was purchased from Avanti Polar Lipids (Alabaster, AL, USA). Iron (III) acetylacetonate [$Fe(acac)_3$] (99.9+%), 1,2-hexadecanediol (90%), oleic acid (90%), oleylamine (70%), phenyl ether ($C_{12}H_{10}O$), ferric chloride ($FeCl_3.6H_2O$), potassium thiocynate (KSCN), hydrogen peroxide (H_2O_2) was purchased from Sigma-Aldrich, Inc. (St. Louis, MO, USA), FragEL™ DNA Fragmentation Detection Kit, Fluorescent - TdT Enzyme was purchased from EMD Millipore (Billerica, MA. USA). Cell lines were purchased from the American Type Culture Collection (Rockville, MD, USA). Cell culture media, Dulbecco's Modified Eagle's medium (DMEM), Hanks' balanced salt solution (HBSS), fetal bovine serum (FBS), and penicillin/streptomycin stock solutions were purchased from CellGro (Kansas City, MO, USA). Reverse osmosis-derived and deionized water (D.I. water) were used in all experiments.

Preparation of micelles

Theranostic micelles were prepared by the lipid film rehydration method [11] as follows; 10 mg of PEG–PE in chloroform, 1 to 5 % w/w of SPIONs in chloroform and 1.5 % w/w Paclitaxel (PTX) (1mg/ml methanol) were mixed together in a glass vial. The organic solvents were removed by rotary evaporation or by rotation under N_2 gas for 10 mins or until any visible solvents were removed at room temperature. Residual solvents were removed by freeze-drying overnight. The dry film obtained was rehydrated with 1 mL (for *in vitro* use) or 0.15 mL (for *in vivo* use) of 10 mM HEPES-buffered saline (HBS) pH 7.4 and vortexed vigorously to produce micelles. Excess non-incorporated drug and/or contrast agent were separated by centrifugation (13,000 × g) for 10 mins to leave PTX-SPION-loaded PEG–PE (theranostic) micelles in the supernatant. For comparisons, controls including SPION-PEG–PE (SPION) micelles, PTX-PEG–PE (PTX) micelles and PEG–PE (plain) micelles were also prepared by the lipid film rehydration method. Following preparation of these formulations, they were used within the period of 72 hrs.

Magnetic resonance imaging

MR images were obtained at ambient temperature (~ 25°C) using a Bruker Biospec 7.0T/20-cm USR horizontal magnet (Bruker, Billerica, MA, USA) and a 20-G/cm magnetic field gradient insert (ID =12cm) capable of a 120-μs rise time (Bruker). Briefly, micelles samples were placed in a 96-well plate and covered with plastic film. The plate was placed in the magnet and radiofrequency signals were sent and received with the quad electronics (INSL, Leominster, MA, USA). A T2-weighted image was acquired using a multi-slice multi-echo (MSME) pulse sequence. The echo time (TE) was 11 ms, and 16 echoes were acquired during imaging with a recovery time (TR) of 2500 ms. Images were acquired with a field of view (FOV) = 4 × 4 cm^2, data matrix = 256 × 256, slice thickness = 2 mm, and 2 signal averages.

For *in vivo* studies, mice were placed in the magnet under constant flow of 2% isoflurane for the duration of imaging. Respiration rate was monitored throughout the scan. A T2-weighted image was acquired using a MSME pulse sequence. The TE, was 22 ms, and 16 echoes were acquired during imaging with a TR of 2500 ms. Images were acquired with a FOV = 4 × 4 cm^2, data matrix = 256 × 256, slice thickness = 1 mm with 2 signal averages.

T2 relaxation time measurements

T2 relaxation values were obtained from a region of interest (ROI) in areas of the T2-weighted image obtained using ParaVison 5.1 software. The T2 values were automatically computed using the equation; y=A+C*exp(-t/T2) (S.D. weighted). Where, A = Absolute bias, C = signal intensity, t = echo time and T2 = spin-spin relaxation time.

Cell cultures

The murine mammary carcinoma 4T1 and murine melanoma B16F10 cells (American Type Culture Collection, Manassas, VA, USA) were grown and maintained in DMEM culture medium at 37°C, 5% CO_2. DMEM was supplemented with 10% FBS, 1 mM Na-pyruvate, 50U/mL penicillin, and 50 μg/ml streptomycin.

Cytotoxicity assay

Cytotoxicity of micelles was evaluated using a CellTiter 96® AQ_{ueous} Non-reactive cell proliferation assay (Promega, Madison, WI USA). Briefly, 4T1 or B16F10 cells were plated at a density of 5×10^3 cells per well in 96-well plates (Corning Inc., Corning, NY, USA). After 24 hours incubation at 37°C, 5% CO_2, the medium was replaced with medium containing free drug dissolved in methanol at a concentration ranging from 4.68 to 600 ng/ml or PTX-PEG–PE micelles or theranostic micelles or SPION-PEG-PE micelles or empty PEG-PE micelles. As a supplementary control, methanol was used at a concentration of 0.012% v/v. After an additional 24 or 48 hour incubation at 37°C, 5% CO_2, micelle and free-drug containing media was removed. Each well was washed twice with DMEM and cell viability determined by measurement of the fluorescence intensity with excitation/emission wavelengths of 525/590 nm using a BioTek Synergy HT multimode microplate reader (BioTek Instruments, Winooski, VT, USA).

Animal models

All animal experiments were conducted as per an animal protocol approved by The Division of Laboratory Animal Medicine and Northeastern University's Institutional Animal Care and Use Committee. We used two mouse tumor models. Approximately 1.5×10^5 4T1 or B16F10 cells (100 μl PBS, pH 7.4) were inoculated in 6–8 weeks-old female Balb/C mice and 6–8 weeks-old male C57BL/6 mice respectively by the subcutaneous injection into the left flank. Prior to injection of cells, mice were anesthetized with 1.5% isoflurane and depilated around the trunk. Fourteen days after tumor inoculation, when the tumor volumes reached 150 to 200 mm^3, the mice were injected intratumorally with different formulations equivalent to 5mg/kg of PTX. After 48 hrs, the tumors were harvested, embedded in tissue freezing media and stored at −80°C until further analysis.

Microscopic analysis of tissue samples

Tumor tissues were sectioned as 4-μm-thick sections using a freezing microtome and mounted onto glass slides (Superfrost Plus®, ThermoFisher Scientific, Waltham, MA, USA). Sections were stained using the Terminal Deoxynucleotidyl Transferase Biotin-dUTP Nick End Labeling (TUNEL) assay kit for apoptosis using the manufacturer's protocol. SPION particles were identified in the tumor tissue using a HT20 Iron Staining kit (Sigma-Aldrich, St. Louis, MO, USA).

RESULTS

To form the theranostic agent, PTX and SPIONs were solublized in the micelle core (Figure 1A). The average size for empty PEG-PE micelles was about 16 nm in diameter, with a size range of 12 – 20 nm using dynamic light scattering (Figure 1B). Loading micelles with SPIONs, PTX or both SPIONs and PTX had no significant effect on the average size or size distribution pattern.

Further, we investigated the presence of SPIONs by Transmission electron microscopy (TEM) analysis. Negative staining with 2% phosphotungstic acid confirmed the presence of SPIONs in both SPION-micelles and theranostic micelles (Figure 1C). Both micelle formulations had a dark core of SPIONs, encircled by an unstained micellar corona with a thickness of 2–3 nm. Plain micelles and PTX-micelles lacked such a dark core. The diameter of the micelles determined by TEM ranged from 10 to 15 ± 2.2 nm, which was in agreement with particle size analysis using dynamic light scattering.

Further, the amount of PTX and SPIONs within the micelles was quantified. The amount of PTX solublized in the micelles was determined by reversed phase HPLC (Figure S1A Supporting Information). Relative to the initial amount of PTX (0.150 mg/ml), about 96 % incorporation was achieved in PTX-micelles (0.144 mg/ml). When compared to theranostic micelles, no significant difference in the PTX loading was observed in the presence of SPIONs. The micelles were further characterized for their iron-content (Figure S1B Supporting Information), since they must possess a sufficient SPION load in order to respond an external magnetic field. The iron content increased nearly linearly as SPION concentration was increased from 1 to 5% (Figure S1C Supporting Information). The iron

content in the theranostic micelles equaled the iron content of SPION-micelles (0.06 mg/ml). About 70 % incorporation was achieved in both SPION and theranostic micelles.

SQUID analysis for each preparation was carried out at 300°K to determine their magnetic susceptibility (Figure S3 Supporting Information). A typical hysteresis curve was obtained with a high saturation magnetization value for SPION-micelles (2.0×10^{-5} emu) and theranostic micelles (1.5×10^{-5} emu) compared to plain micelles (0.25×10^{-5} emu) and PTX-micelles (0.5×10^{-5} emu). The absence of a hysteresis loop indicated that the SPION-micelles and theranostic micelles exhibited superparamagnetic behavior and so were further tested for their MRI properties.

MRI was used to observe the T2-weighted images of various concentrations of SPION-micelles with/without PTX. The formulations containing SPION produced a darker image compared to the non-SPION controls and D.I. water used as a reference (Figure 2A) indicating T2-transverse contrast. The addition of the PTX (Figure 2B) did not affect the T2-weighted imaging.

The contrast observed was SPION-concentration dependent in both cases. Further, the T2 relaxation times confirmed that increasing the amounts of contrast agent decreased the relaxation time. This was also observed when PTX was added to SPION-micelles. (Figure 2D). The contrast properties with theranostic micelles were comparable to those of drug-free SPION-micelles (Figure 2C). The T2 relaxation time of the micelles, (Figure 2E), decreased significantly with incorporation of SPIONs and remained unchanged in the presence of PTX.

Some concern has been associated with the possible toxicity of SPIONs. To evaluate the potential toxicity of formulations, 4T1 and B16F10 cell viability was assessed after treatments. SPION-micelles (1 to 5 % w/w) had no effect on the cell viability after incubation for 24, 48 or 72 hours of either cell line (Figure S4 Supporting Information). Likewise, no significant cytotoxicity was observed with plain PEG-PE micelles. In the presence of free PTX, PTX-micelles and theranostic micelles, a 20 % decrease in cell viability was observed in both cell lines after 24 hours incubation tested at all PTX concentrations (Figure 3A, 3B). SPION-micelles were not toxic.

They had no apparent anti-cancer effects at a SPION concentration of 0.015 to 0.25 μg/mL. No differences in cytotoxicity were observed among the free PTX, PTX- micelles, and theranostic micelles. However, after 48 hours of incubation, a clear difference among free PTX and PTX-micelles and theranostic micelles occurred (Figure 3C, 3D). The micellar preparations showed increased toxicity. Up to a 30 to 40% decrease in cell viability was observed with free drug in 4T1 and B16F10 cells and as much as a 60 % decrease in cell viability was seen with PTX-micelles and theranostic micelles in both cell lines. This data also suggests that presence of SPIONS did not alter the cytotoxic potential of PTX within the theranostic micelles.

After *in vitro* characterization of the theranostic micelles, their imaging properties were compared to SPION micelles *in vivo*. Following intratumoral injection, both breast and melanoma (Figure 4A, 4B) tumor-bearing mice demonstrated an enhancement of the T-2

weighted image contrast. The *in vivo* MR images were clearly distinguishable pre- and post-injection of theranostic micelles in both tumor models.

The MR images with theranostic and SPION micelles were highly contrasted. Color-coded composite images confirmed the MR images. The high T2 activity observed post-injection of contrast agents indicated the T2 intensity values corresponding to the contrast agent present. The images were obtained following a dose of 100μl of SPIONs (equivalent to 3mg of Fe/Kg). Theranostic micelles produced a contrast similar to SPION micelles. This remained apparent with MR imaging after 72 hours (Figure 4C). These results indicate that theranostic micelles retain their imaging property *in vivo* for up to 72 hours and that this property is unaffected by the presence of PTX. These results agree with our *in vitro* studies that showed no difference in the imaging properties between theranostic and SPION-only micelles.

Histological analysis confirmed the presence of SPION particles in both *in vivo* tumor cell models. Prussian blue staining (Figure 5A) revealed clusters of iron particles in tumors of mice treated with both theranostic and SPION micelles. This was not observed in mice treated with either plain or PTX micelles. Similar clusters were observed 72 hours after injection (Figure 5B).

Apoptotic activity of the theranostic agent was evaluated in both tumor models by TUNEL assay and quanified, (Figure 6). Nuclei were stained with DAPI, and apoptotic cells were fluorescently labeled green. The presence of apoptosis or nuclear DNA fragmentation in tumor sections confirmed similar levels of apoptotic cell death in mice treated with PTX and theranostic micelles in both tumor types at 24 hours (Figure 6A, 6B). The apoptotic activity of drug encorporated micelles (PTX and theranostic) continued for up to 72 hours (Figure 6C, 6D). The average Fluorescence Intensity (F.I) for 24 and 72 hours were quantified and expressed as (arbitrary units) (Figure 6E). For Plain and SPION micelles the average F.I was 1.04±0.42 and 0.31±0.12 respectively. While, for PTX and Theranostic micelles, the average F.I increased to 10.76±0.97 and 12.29±1.23 respectively. The images indicate that these theranostic micelles effectively promote cancer cell death *in vivo*.

DISCUSSION

Interest in the combination of a diagnostic and therapeutic agent to form a theranostic system for improved treatment and detection of cancer has continued to grow. The use of a contrast agent as a part of a therapeutic preparation allows imaging before, during and after treatment and thereby provides a more useful and personalized form of chemotherapy by bridging the gap between cancer diagnosis and therapy [7]. Theranostic agents are prepared by either by chemical immobilization of drug molecules or electrostatic coupling, however these modifications are restricted to surface chemistry. Additionally, most of the current SPION-containing theranostic agents have been prepared using doxorubicin (DOX) [12–27]. Given that many chemotherapeutic and contrast agents possess poor water solubility, we encapsulated both poorly soluble PTX and hydrophobic SPIONs simultaneously in a polymeric PEG-PE micelle. One of the main goals is to provide as a platform of

development of novel theranostic agents incorporating hydrophobic drugs and contrast agents.

Our initial formulation optimization was carried out by varying the percent by weight of SPION to the weight of PEG-PE (1 to 5% w/w) to prepare SPION micelles. These micelles were of uniform size [28] and could be entrapped within the micelle core together with PTX. In some cases, micelle size ranging from 17 to 110 nm has been reported [29], due the difference in the particle size of IONs themselves. Theranostic micelles were prepared by incorporating 1.5% w/w of PTX in SPION containing micelles [30]. The addition of PTX had no effect on particle size. We confirmed the presence of SPIONs by TEM analysis. The corona around the dark electron-dense core of ION indicated the incorporation of SPION particles within the micelle core, as was reported previously [31, 32].

The amount of iron within the micelles was quantified using a modified version of iron-content estimation technique [33]. We observed a trend towards saturation, indicating the limitation of solublization of SPION within the micelle core as evident by a decrease in incorporation efficiency as the SPION concentration increased. This tendency is due to the limited hydrophobic area available for SPION solublization and is in good agreement with other data indicating similar behavior as the SPION concentrations were increased [34]. No difference in the iron content of the theranostic micelles and SPION-micelles was observed, indicating that the micelles just as fully solublized the contrast agent both in the presence and absence of the drug. Similarly, PTX loading in theranostic micelles was unaltered due to the presence of SPIONs.

Most importantly, the SPION load within the theranostic micelles was sufficient for imaging. This was was evident from the high saturation magnetization of SPION-micelles and theranostic micelles, during SQUID analysis, that were found to be attributable to the presence of the SPIONs, as reported by others [35–37]. Plain micelles and PTX-micelles showed a pattern similar to diamagnetic materials with minimal background. The absence of the hysteresis loop in the case of SPION-micelles and theranostic micelles confirmed the superparamagnetic behavior of SPIONs and their potential usefulness for MRI application for further studies.

Formulations were imaged to determine their imaging properties. Contrast obtained during a MRI was due to the iron oxide nanoparticles that typically generate intravoxel dephasing, resulting in decreased signal intensity and enhanced the T2-weighted image contrast. The images of formulations containing SPION micelles clearly demonstrated loss of the signal intensity in a concentration-dependent fashion at 1 to 5% w/w SPIONS. Similarly, other groups reported that an increase in the IONs from 16.25 uM to 1040 uM in 1,2-diacyl-sn-glycero-3-phosphoethanolamine-N-[methoxy(polyethylene glycol)-5000] DSP-PEG5K micelles increased the signal intensity observed from the T2-weighted image [29]. Importantly, no changes in signal intensity were observed when 1.5% w/w paclitaxel was added to SPION-containing micelles, indicating that the addition of PTX does not affect the MRI or T2 relaxation parameters. The high T2 relaxation time in non-SPION containing formulations is due to the rapid movement of hydrogen atoms in the water that experience only a uniform magnetic environment resulting in a very long T2 relaxation time [38]

making it hard to visualize contrast. In the presence of the SPION contrast agent the T2 relaxation time shortened, producing an enhanced contrast, without any interference by PTX in the MRI signal.

The histogram shows T2 relaxation time, which is time constant for the magnetic resonance signal to irreversibly decay to 1/e (~37%) of its initial value after 90° pulse. This value is computed by fitting signal intensities at different echo times (10 to 18) to transverse relaxation equation. This T2 value is invariable across the same strength MRI system and varies slightly across different strength MRIs.

Contrary to invariable T2 value the signal intensity of MRI image is function of many variables and T2 value is one of them. The intensity changes based on coil system, position of sample relative to the coil, position of slice in sample, magnetic homogeneity (shimming quality) at the time of imaging etc.; hence for any MR contrast agent the quality is described as a function of T1 or T2 time. The slight variation in signal intensity in Figure 2A and Figure 2B are due to some of above mentioned factors and due to imaging software's automated contrast adjustment based on maximum and minimum pixel intensity in that image.

We further investigated the toxicity of SPION containing formulations. SPIONs alone at 0.005 to 0.8 mg/ml did not influence *in vitro* cell viability of different cancer cells, including MCF-7,[37] LNCap and PC3 [39]. However, at much higher SPION concentrations (500 to 1000 mg/mL), cell viability of MDA-MB-435 decreased to about 40% after 3 days exposure [36]. At the SPION concentration used in our experiments to prepare theranostic micelles (0.015 to 0.25 μg/mL), no decrease in viability of 4T1 or B16F10 cells occurred over a period of 72 hours indicating little likelihood of direct SPION toxicity.

Following *in vitro* characterization, the theranostic fomulations were tested for *in vivo* applicaiton using MRI. Our main goal in this study was to confirm the preservation of a sufficient therapeutic and contrast activity by the micelle-incorporated theranostic agent rather than to develop the actual treatment strategy, that is why we have used a straightforward intratumoral administration of the theranostic preparation. One has to note however, that intratumoral administration on its own is of interest since it is also used as an experimental and clinical strategy to treat cancer [40, 41]. In addition, intratumoral injection minimizes unwanted biodistribution and has various advantages such as diffusion of the formulation limited primarily to the interstitial space within the tumor [42]. This allowed us to study specifically the contrast and therapeutic properties of the theranostic agent. The MR images were clearly distinguishable pre- and post-injection of theranostic micelles in both tumor models. The images with theranostic and SPION micelles were highly contrasted. These results agree with our *in vitro* studies that showed no difference in the imaging properties between theranostic and SPION-only micelles. Similar results were reported when magnetite/silica core-shell nanoparticles were injected intratumorally in a breast tumor model [43] and magnetic cationic liposomes in SCID mice [44], respectively. Some additional contrast was also observed around the tumor interstitium, perhaps due to the relatively high intratumor pressure and the multiple injections of the formulation [45]. The dose of SPIONs in the theranostic micelles administered was equivalent to 3 mg Fe/Kg,

which is much less than the 20 mg Fe/kg of Fe [36] or 12.5 mg Fe/Kg used previously *in vivo* to produce T2-weighted contrast images [46]. Additionally, PTX within our theranostic micelles did not alter the imaging properties.

Further, tissue sections were stained with Prussian blue that confirmed the presence of iron within the tumor tissue after SPION-only and theranostic micelles injections that remained localized. Similarly, iron deposits were observed in sections obtained from pancreatic tumors [47] and from squamous cell carcinomas [48]. Additionally, *in vitro* uptake of iron was observed in LNCaP, PC3 [39] and HeLa [49] cells incubated with SPION particles by positive Prussian blue staining.

The TUNEL assay identified and differentiated apoptotic from necrotic cells by the presence of DNA fragmentation that is produced by apoptotic cells and confirmed by labeling with Fluorescein FragEL™ [50]. Following quantification of TUNEL assay, we observed no significant differences in the levels of apoptotic cell death between mice treated with PTX and theranostic micelles after 48 and 72 hours in both mouse tumor models, while only background fluorescence was observed in plain or SPION-micelles treated mice with absence of apoptosis. Similar results were observed in a breast tumor model when mice received intratumoral injections of PTX micelles [51]. Both our *in vivo* and *in vitro* cytotoxicity results confirmed that the presence of SPIONs within the theranostic agent was not itself toxic and did not interfere with the cytotoxic properties of PTX.

CONCLUSIONS

In summary, the theranostic agent described here, readily incorporates both PTX and SPIONs and simultaneously allows for diagnostic imaging and apoptotic anti-tumor activity. The active agents were optimally accommodated within a micelle core without alteration in micelle properties or the functional activity of either. These theranostic micelles provided an excellent T2-weighted contrast MR signal in vivo, which was confirmed by histological studies showing good localization of SPION as well as significatnly increased apoptosis in the tumor tissue. The advantages of the theranostic approach include the provision for early feedback about the therapeutic efficacy of a chemotherapeutic agent. The use of such theranostic agents should help to overcome some of the current challenges associated with a “one-size-fits-all” form of chemotherapy and lead to a more effective personalized treatment. The synergy of such a theranostic agent will enable an efficient evaluation of the preclinical properties of the drug. Unlike conventional ex vivo analysis that are labor intensive and time consuming, similar information can be obtained in real-time using imaging techniques. Drug delivery with a simultaneous imaging will enable the visualization of the active agent accumulation in the specific target as well as its biological effect. For example, it could play a crucial role in performing site-specific radiation-based therapies, such as radiotherapy, hyperthermia and photodynamic therapy.

Supplementary Material

Refer to Web version on PubMed Central for supplementary material.

Acknowledgments

This work was supported by the NIH grant 1RO1CA121838 and 1U54CA151881 to V. P. Torchilin. We thank W. H. Fowle, at the Electron Microscopy Center, Department of Biology, Northeastern University for his technical support in use of the JOEL JEM-1010 Transmission Electron Microscope. We also thank W. C. Hartner for his editorial assistance in preparation of this manuscript.

References

1. Rai P, Mallidi S, Zheng X, Rahmanzadeh R, Mir Y, Elrington S, Khurshid A, Hasan T. Development and applications of photo-triggered theranostic agents. Adv Drug Deliv Rev. 2010; 62(11):1094–124. [PubMed: 20858520]
2. MacKay JA, Li Z. Theranostic agents that co-deliver therapeutic and imaging agents? Adv Drug Deliv Rev. 2010; 62(11):1003–4. [PubMed: 20937334]
3. Maeda H, Wu J, Sawa T, Matsumura Y, Hori K. Tumor vascular permeability and the EPR effect in macromolecular therapeutics: a review. J Control Release. 2000; 65(1–2):271–84. [PubMed: 10699287]
4. Khemtong C, Kessinger CW, Gao J. Polymeric nanomedicine for cancer MR imaging and drug delivery. Chem Commun. 2009; (24):3497–510.
5. Hahn MA, Singh AK, Sharma P, Brown SC, Moudgil BM. Nanoparticles as contrast agents for in-vivo bioimaging: current status and future perspectives. Anal Bioanal Chem. 2011; 399(1):3–27. [PubMed: 20924568]
6. Sawant R, Sawant R, Gultepe E, Nagesha D, Papahadjopoulos-Sternberg B, Sridhar S, Torchilin V. Nanosized cancer cell-targeted polymeric immunomicelles loaded with superparamagnetic iron oxide nanoparticles. J Nanopart Res. 2009; 11(7):1777–1785.
7. Xie J, Lee S, Chen X. Nanoparticle-based theranostic agents. Adv Drug Deliv Rev. 2010; 62(11): 1064–79. [PubMed: 20691229]
8. Weissleder R, Stark D, Engelstad B, Bacon B, Compton C, White D, Jacobs P, Lewis J. Superparamagnetic iron oxide: pharmacokinetics and toxicity. Am J Roentgenol. 1989; 152(1):167. [PubMed: 2783272]
9. Weissleder R, Pittet MJ. Imaging in the era of molecular oncology. Nature. 2008; 452(7187):580–9. [PubMed: 18385732]
10. Wu EX, Tang H, Jensen JH. Applications of ultrasmall superparamagnetic iron oxide contrast agents in the MR study of animal models. NMR Biomed. 2004; 17(7):478–83. [PubMed: 15526349]
11. Sawant RR, Torchilin VP. Polymeric micelles: polyethylene glycol-phosphatidylethanolamine (PEG-PE)-based micelles as an example. Methods Mol Biol. 2010; 624:131–49. [PubMed: 20217593]
12. Yang X, Grailer JJ, Rowland IJ, Javadi A, Hurley SA, Matson VZ, Steeber DA, Gong S. Multifunctional stable and pH-responsive polymer vesicles formed by heterofunctional triblock copolymer for targeted anticancer drug delivery and ultrasensitive MR imaging. ACS Nano. 2010; 4(11):6805–17. [PubMed: 20958084]
13. Park JH, von Maltzahn G, Ruoslahti E, Bhatia SN, Sailor MJ. Micellar hybrid nanoparticles for simultaneous magnetofluorescent imaging and drug delivery. Angew Chem Int Ed Engl. 2008; 47(38):7284–8. [PubMed: 18696519]
14. Nasongkla N, Bey E, Ren J, Ai H, Khemtong C, Guthi JS, Chin SF, Sherry AD, Boothman DA, Gao J. Multifunctional polymeric micelles as cancer-targeted, MRI-ultrasensitive drug delivery systems. Nano Lett. 2006; 6(11):2427–30. [PubMed: 17090068]
15. Kaaki K, Herve-Aubert K, Chiper M, Shkilnyy A, Souce M, Benoit R, Paillard A, Dubois P, Saboungi ML, Chourpa I. Magnetic nanocarriers of doxorubicin coated with poly(ethylene glycol) and folic acid: relation between coating structure, surface properties, colloidal stability, and cancer cell targeting. Langmuir: the ACS journal of surfaces and colloids. 2012; 28(2):1496–505. [PubMed: 22172203]

16. Sun Q, Cheng D, Yu X, Zhang Z, Dai J, Li H, Liang B, Shuai X. A pH-sensitive polymeric nanovesicle based on biodegradable poly(ethylene glycol)-b-poly(2-(diisopropylamino)ethyl aspartate) as a MRI-visible drug delivery system. J Mater Chem. 2011; 21(39):15316–15326.
17. Ren T, Liu Q, Lu H, Liu H, Zhang X, Du J. Multifunctional polymer vesicles for ultrasensitive magnetic resonance imaging and drug delivery. J Mater Chem. 2012; 22(24):12329–12338.
18. Chen D, Xia X, Gu H, Xu Q, Ge J, Li Y, Li N, Lu J. pH-responsive polymeric carrier encapsulated magnetic nanoparticles for cancer targeted imaging and delivery. J Mater Chem. 2011; 21(34): 12682–12690.
19. He X, Wu X, Cai X, Lin S, Xie M, Zhu X, Yan D. Functionalization of magnetic nanoparticles with dendritic-linear-brush-like triblock copolymers and their drug release properties. Langmuir: the ACS journal of surfaces and colloids. 2012; 28(32):11929–38. [PubMed: 22799877]
20. Purushotham S, Chang PE, Rumpel H, Kee IH, Ng RT, Chow PK, Tan CK, Ramanujan RV. Thermoresponsive core-shell magnetic nanoparticles for combined modalities of cancer therapy. Nanotechnology. 2009; 20(30):305101. [PubMed: 19581698]
21. Rastogi R, Gulati N, Kotnala RK, Sharma U, Jayasundar R, Koul V. Evaluation of folate conjugated pegylated thermosensitive magnetic nanocomposites for tumor imaging and therapy. Colloids SurfB. 2011; 82(1):160–7.
22. Wu X, He X, Zhong L, Lin S, Wang D, Zhu X, Yan D. Water-soluble dendritic-linear triblock copolymer-modified magnetic nanoparticles: preparation, characterization and drug release properties. J Mater Chem. 2011; 21(35):13611–13620.
23. Kim B, Peppas NA. Synthesis and characterization of pH-sensitive glycopolymers for oral drug delivery systems. J Biomater Sci Polym Ed. 2002; 13(11):1271–81. [PubMed: 12518804]
24. Yang X, Grailer JJ, Rowland IJ, Javadi A, Hurley SA, Steeber DA, Gong S. Multifunctional SPIO/DOX-loaded wormlike polymer vesicles for cancer therapy and MR imaging. Biomaterials. 2010; 31(34):9065–73. [PubMed: 20828811]
25. Sanson C, Diou O, Thevenot J, Ibarboure E, Soum A, Brulet A, Miraux S, Thiaudiere E, Tan S, Brisson A, Dupuis V, Sandre O, Lecommandoux S. Doxorubicin loaded magnetic polymersomes: theranostic nanocarriers for MR imaging and magneto-chemotherapy. ACS Nano. 2011; 5(2): 1122–40. [PubMed: 21218795]
26. Andhariya N, Chudasama B, Mehta R, Upadhyay R. Biodegradable thermoresponsive polymeric magnetic nanoparticles: a new drug delivery platform for doxorubicin. J Nanopart Res. 2011; 13(4):1677–1688.
27. Anirudhan TS, Sandeep S. Synthesis, characterization, cellular uptake and cytotoxicity of a multi-functional magnetic nanocomposite for the targeted delivery and controlled release of doxorubicin to cancer cells. J Mater Chem. 2012; 22(25):12888–12899.
28. Nagesha DK, Plouffe BD, Phan M, Lewis LH, Sridhar S, Murthy SK. Functionalization-induced improvement in magnetic properties of Fe3O4 nanoparticles for biomedical applications. J Appl Phys. 2009; 105(7):07B317-07B317-3.
29. Ai H, Flask C, Weinberg B, Shuai XT, Pagel MD, Farrell D, Duerk J, Gao J. Magnetite-Loaded Polymeric Micelles as Ultrasensitive Magnetic-Resonance Probes. Adv Mater. 2005; 17(16):1949–1952.
30. Gao Z, Lukyanov A, Singhal A, Torchilin V. Diacylipid-polymer micelles as nanocarriers for poorly soluble anticancer drugs. Nano Lett. 2002; 2:979–982.
31. Nitin N, LaConte LE, Zurkiya O, Hu X, Bao G. Functionalization and peptide-based delivery of magnetic nanoparticles as an intracellular MRI contrast agent. J Biol Inorg Chem. 2004; 9(6):706–12. [PubMed: 15232722]
32. Xie J, Liu G, Eden HS, Ai H, Chen X. Surface-Engineered Magnetic Nanoparticle Platforms for Cancer Imaging and Therapy. Acc Chem Res. 2011
33. Cengelli F, Maysinger D, Tschudi-Monnet F, Montet X, Corot C, Petri-Fink A, Hofmann H, Juillerat-Jeanneret L. Interaction of functionalized superparamagnetic iron oxide nanoparticles with brain structures. J Pharmacol Exp Ther. 2006; 318(1):108–16. [PubMed: 16608917]
34. Talelli M, Rijcken CJ, Lammers T, Seevinck PR, Storm G, van Nostrum CF, Hennink WE. Superparamagnetic iron oxide nanoparticles encapsulated in biodegradable thermosensitive

polymeric micelles: toward a targeted nanomedicine suitable for image-guided drug delivery. Langmuir. 2009; 25(4):2060–7. [PubMed: 19166276]

35. Chandrasekharan P, Maity D, Yong CX, Chuang KH, Ding J, Feng SS. Vitamin E (d-alpha-tocopheryl-co-poly(ethylene glycol) 1000 succinate) micelles-superparamagnetic iron oxide nanoparticles for enhanced thermotherapy and MRI. Biomaterials. 2011; 32(24):5663–72. [PubMed: 21550654]
36. Gao GH, Lee JW, Nguyen MK, Im GH, Yang J, Heo H, Jeon P, Park TG, Lee JH, Lee DS. pH-responsive polymeric micelle based on PEG-poly(beta-amino ester)/(amido amine) as intelligent vehicle for magnetic resonance imaging in detection of cerebral ischemic area. J Control Release. 2010
37. Dilnawaz F, Singh A, Mohanty C, Sahoo SK. Dual drug loaded superparamagnetic iron oxide nanoparticles for targeted cancer therapy. Biomaterials. 2010; 31(13):3694–706. [PubMed: 20144478]
38. Hendrick, RE. Breast MRI: fundamentals and technical aspects. Springer Verlag; 2007.
39. Wang AZ, Bagalkot V, Vasilliou CC, Gu F, Alexis F, Zhang L, Shaikh M, Yuet K, Cima MJ, Langer R, Kantoff PW, Bander NH, Jon S, Farokhzad OC. Superparamagnetic iron oxide nanoparticle-aptamer bioconjugates for combined prostate cancer imaging and therapy. ChemMedChem. 2008; 3(9):1311–5. [PubMed: 18613203]
40. Grassi G, Grassi M. First-in-human trial of Dz13 for nodular basal-cell carcinoma. Lancet. 2013; 381(9880):1797–8. [PubMed: 23660122]
41. Cho E-A, Moloney FJ, Cai H, Au-Yeung A, China C, Scolyer RA, Yosufi B, Raftery MJ, Deng JZ, Morton SW, Hammond PT, Arkenau H-T, Damian DL, Francis DJ, Chesterman CN, Barnetson RSC, Halliday GM, Khachigian LM. Safety and tolerability of an intratumorally injected DNAzyme, Dz13, in patients with nodular basal-cell carcinoma: a phase 1 first-in-human trial (DISCOVER). Lancet. 2013; 381(9880):1835–1843. [PubMed: 23660123]
42. Torchilin, VP. Nanoparticulates as Drug Carriers. Imperial College Press; London, UK: 2006. p. 756
43. Campbell JL, Arora J, Cowell SF, Garg A, Eu P, Bhargava SK, Bansal V. Quasi-cubic magnetite/silica core-shell nanoparticles as enhanced MRI contrast agents for cancer imaging. PLoS One. 2011; 6(7):e21857. [PubMed: 21747962]
44. Gultepe E, Reynoso FJ, Jhaveri A, Kulkarni P, Nagesha D, Ferris C, Harisinghani M, Campbell RB, Sridhar S. Monitoring of magnetic targeting to tumor vasculature through MRI and biodistribution. Nanomedicine (Lond). 2010; 5(8):1173–82. [PubMed: 21039195]
45. Jain RK. Barriers to drug delivery in solid tumors. Sci Am. 1994; 271(1):58–65.
46. Yu MK, Jeong YY, Park J, Park S, Kim JW, Min JJ, Kim K, Jon S. Drug-loaded superparamagnetic iron oxide nanoparticles for combined cancer imaging and therapy in vivo. Angew Chem Int Ed Engl. 2008; 47(29):5362–5. [PubMed: 18551493]
47. Gang J, Park SB, Hyung W, Choi EH, Wen J, Kim HS, Shul YG, Haam S, Song SY. Magnetic poly epsilon-caprolactone nanoparticles containing Fe3O4 and gemcitabine enhance anti-tumor effect in pancreatic cancer xenograft mouse model. J Drug Target. 2007; 15(6):445–53. [PubMed: 17613663]
48. Alexiou C, Schmid R, Jurgons R, Kremer M, Wanner G, Bergemann C, Huenges E, Nawroth T, Arnold W, Parak F. Targeting cancer cells: magnetic nanoparticles as drug carriers. European biophysics journal: EBJ. 2006; 35(5):446. [PubMed: 16447039]
49. Huang HC, Chang PY, Chang K, Chen CY, Lin CW, Chen JH, Mou CY, Chang ZF, Chang FH. Formulation of novel lipid-coated magnetic nanoparticles as the probe for in vivo imaging. J Biomed Sci. 2009; 16:86. [PubMed: 19772552]
50. Gold R, Schmied M, Giegerich G, Breitschopf H, Hartung HP, Toyka KV, Lassmann H. Differentiation between cellular apoptosis and necrosis by the combined use of in situ tailing and nick translation techniques. Lab Invest. 1994; 71(2):219–25. [PubMed: 8078301]
51. Sawant RR, Torchilin VP. Enhanced cytotoxicity of TATp-bearing paclitaxel-loaded micelles in vitro and in vivo. Int J Pharm. 2009; 374(1–2):114–8. [PubMed: 19446767]

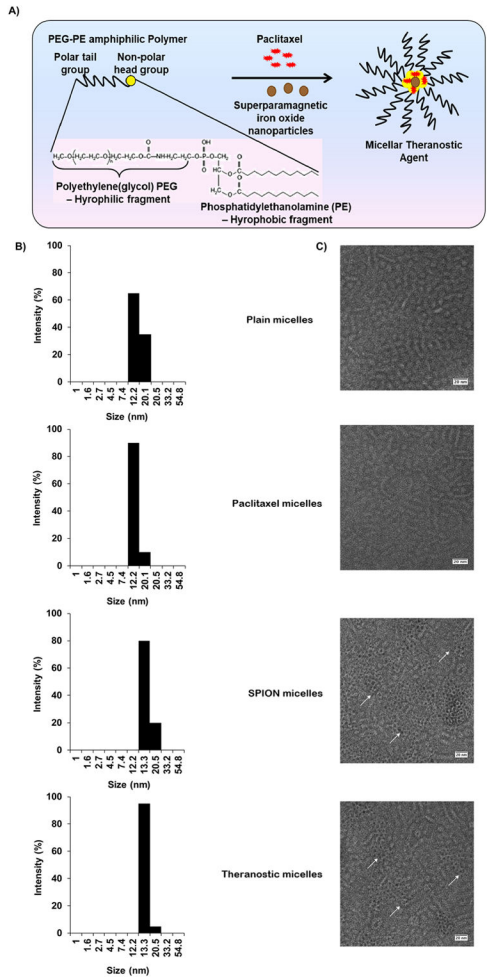

Figure 1. Characterization of micellar theranostic agent

Scheme (A) illustrates a PEG-PE micellar theranostic agent co-incorporated with paclitaxel and MRI contrast agents along with the chemical structure of PEG-PE showing the hydrophilic PEG which depicts the micelle corona and core-hydrophobic PE group, responsible for the solubilization of PTX and entrapment of SPIONs. (B) indicates micelle size and size distribution of empty PEG-PE/Plain micelles, PTX-loaded PEG-PE micelles, SPION-loaded PEG-PE micelles and co-loaded PTX/SPION PEG-PE theranostic micelles with their respective electron micrographs (**C**) at 75,000x magnification, scale bar repesents 100nm. (n=3)

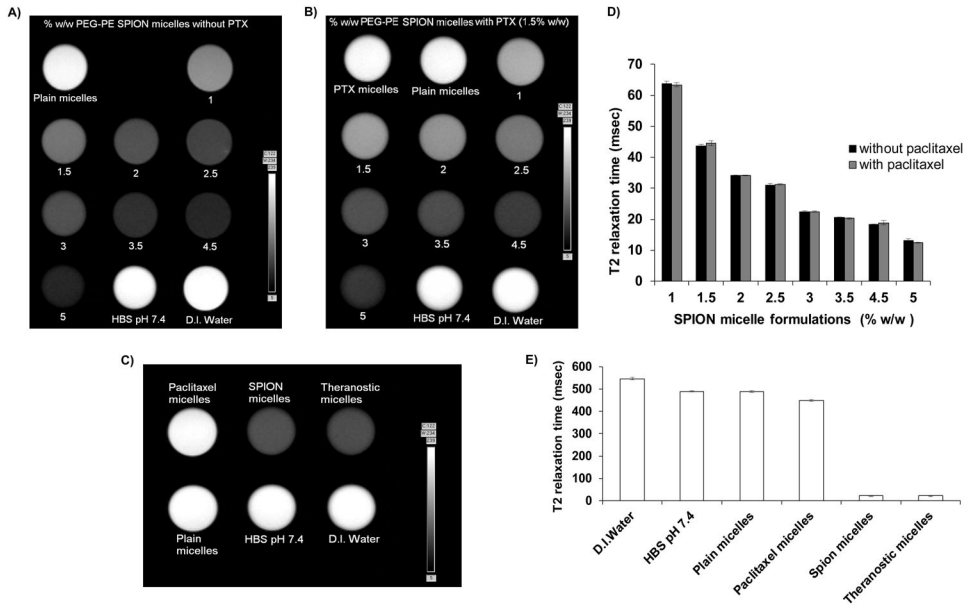

Figure 2. T2-weighted MR image and relaxation times

MR imaging of contrast agent in the absence (A) and presence (B) of 1.5% w/w PTX during formulation optimization and their T2 relaxation times (D). T2-weighted MR images of 3% SPION-containing micelles and controls (C) along with their respective T2 relaxation times (E). MR images were obtained using a 7T Bruker magnet. T2 relaxation times were calculated using Paravision 5.0 software. (mean ± S.D., n=3).

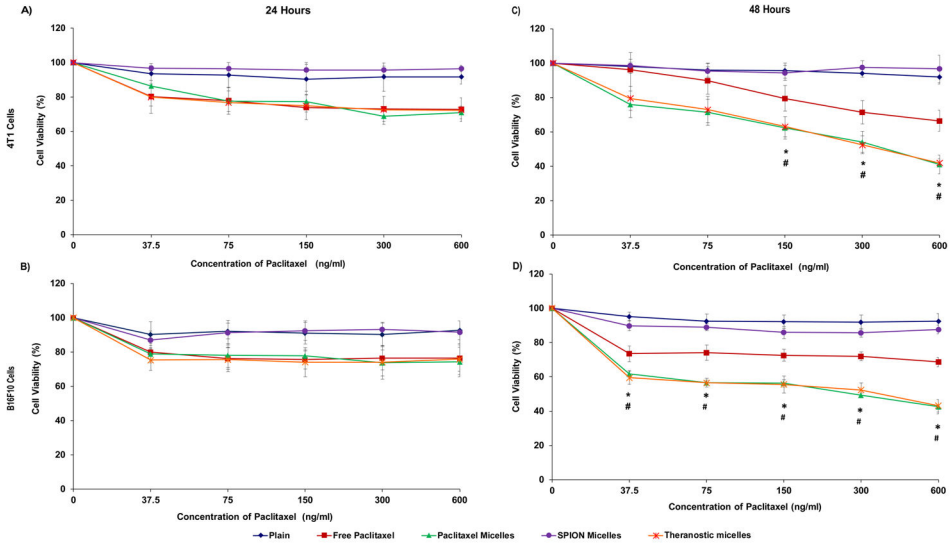

Figure 3. ***In vitro*** **cytotoxicity of micellar formulations**

Percent viability of 4T1 and B16F10 cells after treatment with plain, SPION, PTX, theranostic micelles or free drug (PTX) at +24 hours (A, B) and + 48 hours (C, D) incubation. Data represent mean ± S.D. (n=3). (*) $p < 0.05$ between paclitaxel micelles and free paclitaxel; (#) $p < 0.05$ between theranostic micelles and free paclitaxel (Student's t-test).

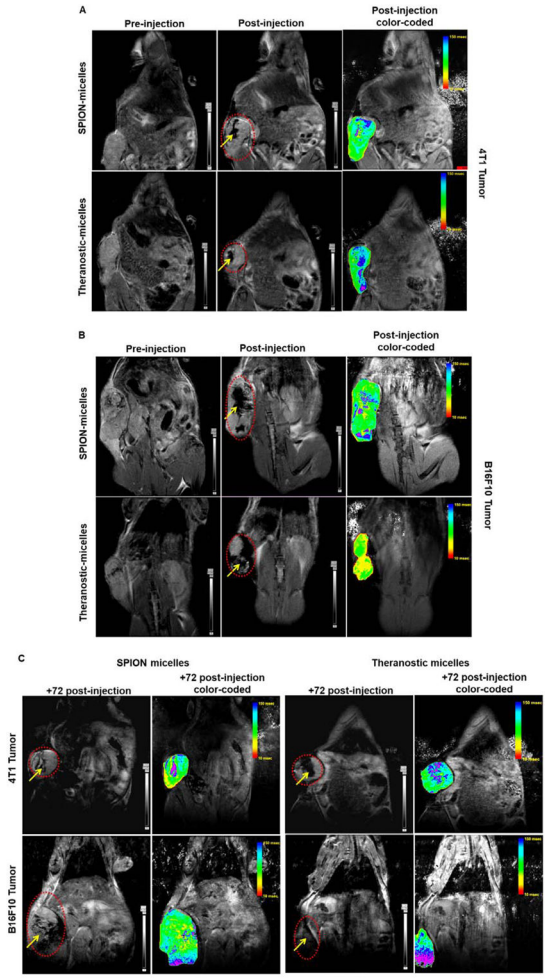

Figure 4. Whole body *in vivo* images

T-2 weighted MR image and color-coded composite maps acquired with breast (A) and melanoma (B) tumor-bearing mice, pre- and post-injection of various formulations containing SPIONs as MR contrast agent. Images were obtained using a 7 Tesla Bruker scanner. Similar images (C) were acquired 72 hours post-injection from both tumor models. Non-color coded images show regions of the tumor bounded by a dotted line. The arrow points the accumulation of contrast agent at the tumor site. Theranostic micelles retained their MR contrast properties equivalent to that of SPION-only micelles.

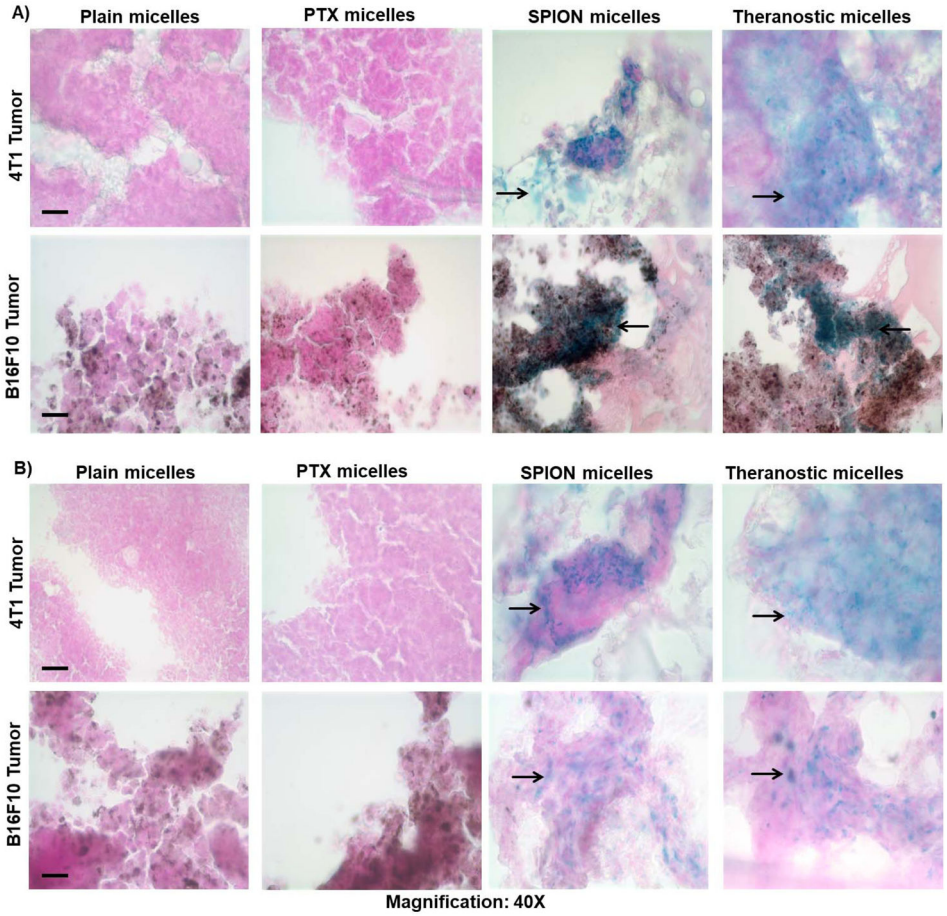

Figure 5. Prussian blue staining of tumor cryosections

Breast (4T1) and melanoma (B16F10) tumor sections stained for SPIONs localized within the tumor interstitium at +48 (A) and +72 hours (B). Blue stain (as indicated by the arrow) from the sections indicates the presence of SPION micelles against a light-red to pink background counterstained with nuclear red that stains cytoplasm and nucleus. The melanoma cells are characterized by their natural dark brown pigments. (*Scale bar = 1cm*)

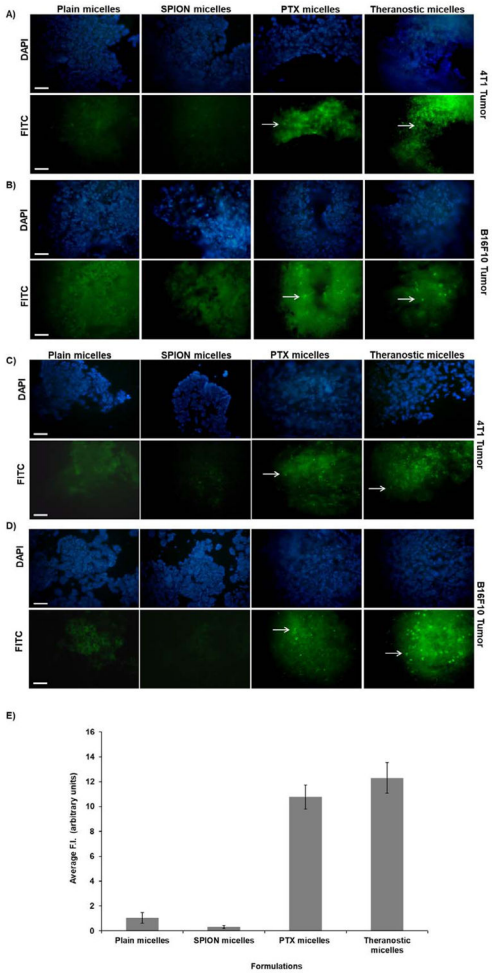

Figure 6. TUNEL assay for apoptotic activity of paclitaxel

In vivo tumor cell apoptosis was induced by intra-tumoral administration of PTX-containing formulations in breast (4T1) and melanoma (B16F10) tumor-bearing mice. At +48 hours (A, B) and +72 hours (C, D) tumor apoptosis was observed after treatment with theranostic and PTX-only-containing formulations as determined by TUNEL assay. Panel (E) shows bar graph of average fluorescence intensity in arbitrary units across all formulations, (n=5) and data is represented as mean±S.D. Cells undergoing apoptosis were observed in the green/FITC channel (see arrow). Sections observed with a blue filter indicate DAPI stain for nuclei. In both cases, tumors treated with plain and SPION micelles lacked DNA fragmenting cells. (*Scale bar = 1cm*).